JOURNAL OF CATALYSIS 134, 36–46 (1992)

Nature and Properties of Pure and Nb-Doped TiO_2 Ceramic Membranes Affecting the Photocatalytic Degradation of 3-Chlorosalicylic Acid as a Model of Halogenated Organic Compounds

J. SABATE,* M. A. ANDERSON,*,[1] H. KIKKAWA,*,[2] Q. XU,* S. CERVERA-MARCH,‡ AND C. G. HILL, JR.†

Water Chemistry Program and †Department of Chemical Engineering, University of Wisconsin, Madison, Wisconsin 53706; and ‡Department of Chemical Engineering, University of Barcelona, Barcelona, Spain 08028

Received April 9, 1991; revised September 9, 1991

Pure and Nb-doped TiO_2 ceramic membranes supported on glass were prepared by sol–gel techniques. When irradiated with near-UV light, these membranes brought about the photocatalytic degradation of 3-chlorosalicylic acid (3-CSA). Relationships between preparation conditions and the characteristics and efficiencies of the different membranes have been inferred. The changes in the physical–chemical characteristics of these membranes when they are fired at high temperatures are retarded by both the Nb-doping and the coating on glass supports. Doping does not improve the rate of degradation of 3-CSA, despite the fact that light absorbance is higher. The increase of firing temperature causes an increase in the size of membrane particles and a remarkable drop in the specific surface area, resulting in a substantial decrease in photochemical efficiency. A discussion based on the hypothesis of e^-/h^+ recombination at grain boundaries and point defects of the membranes is presented.

INTRODUCTION

Illumination of suspensions of semiconductor particles by UV-visible light has been used both to produce nonpolluting fuels like hydrogen (*1–6*) and to degrade organic contaminants present in aqueous streams (*6–11*). In attempts to improve the efficiency of these processes, researchers have investigated both the influence of catalyst properties (chemical nature of the suspended semiconductor, specific surface area, porosity, mean pore size, presence of dopants, etc.) and reaction conditions (pH, temperature, reactant and product concentrations, light intensity, etc.) on the rates of model reactions of these types (*12–16*). Transmission of light in heterogeneous media has also been modeled as one aspect of the design of photochemical reactors (*5, 17*).

In these studies, TiO_2 has been the most commonly employed semiconductor because of its chemical stability. However, it can only absorb light with wavelengths shorter than 400 nm, given the value of 3.2 eV for the bandgap energy of the pure material. In order to utilize a wider range of the electromagnetic spectrum for photocatalysis, researchers have doped TiO_2 to reduce the bandgap energy, added photosensitizers, used semiconductors with smaller bandgap energies (e.g., CdS, Fe_2O_3), and used mixtures of semiconductors (*1, 2, 6, 15, 16*).

When suspensions of TiO_2 particles are used to photodegrade organic contaminants in aqueous systems, the suspended catalyst must be separated from the water to obtain a clean stream. This separation problem

[1] To whom correspondence should be addressed.

[2] Present address: Kure Research Lab., Babcock–Hitachi K.K., No. 3–36, Takara-Machi, Kure-Shi, Hiroshima-Ken, 737 Japan.

0021-9517/92 $3.00

can be avoided by replacing the TiO_2 suspension with a porous coating of TiO_2 on a substrate (*18–20*).

In an earlier study (*21*), TiO_2 ceramic membranes coated on Pyrex glass supports were employed to photodegrade 3-CSA present in aqueous solution. A kinetic study was carried out and a mechanism proposed. 3-CSA was chosen as a model compound for this work because it is a halogenated aromatic compound, which is representative of a wide range of compounds of interest to environmentalists.

Sol–gel techniques used to prepare TiO_2 ceramic membranes provide a vehicle for control of the physical–chemical characteristics of the resulting membrane (*22–25*). In this work, several TiO_2 membranes with different characteristics have been prepared. The photocatalytic properties of these membranes for degrading 3-CSA were investigated with the goal of elucidating how changes in the catalyst preparation procedure influence the properties of the finished catalyst. Two types of membranes have been used: (a) Nb-doped TiO_2 membranes, which should have a lower effective bandgap energy than pure TiO_2 membranes, and (b) pure TiO_2 membranes, in which the mean pore size is modified by changing the colloid preparation conditions.

EXPERIMENTAL

(*i*) *Materials*

Titanium tetraisopropoxide, $NbCl_5$ and 3-chlorosalicyclic acid were obtained from Aldrich Chemical Co. Ethyl alcohol (absolute) was AR grade. All chemicals were used without further purification. The deionized water used in this study was prepared using a Milli-Q water purification system (Millipore Corp.)

(*ii*) *Apparatus*

The photochemical reactor employed has been described elsewhere (*21*). In essence, it is a recirculating flow reactor in which the feedstocks flow through an annulus surrounding a mercury lamp (450 W). TiO_2 (anatase) membranes were supported on the removable inner wall (Pyrex) of the reaction chamber. Reactant solution (1 l) was recirculated between a reservoir and the photochemical reactor. The concentration of dissolved oxygen in the reactant solution was maintained at a constant value by bubbling air into the reactor. The flow rates of the reactant solutions and the air were 210 ml/min and 1000 ml/min, respectively. These rates are sufficient to prevent mass transfer limitations on the observed reaction rate arising from the necessity to transport reactants from the bulk solution to the external surface of the catalytic coating (*21*). The reactor temperature was held at 35°C.

Concentrations of 3-CSA were measured by monitoring the UV absorbance of the solution at 300 nm. Chloride ion and CO_2 concentrations were determined as described elsewhere (*21*). The initial concentration of 3-CSA was always 125 μM. Experiments were conducted at either pH 4.3 or pH 6.

The flux of photons with wavelengths in the range 300–400 nm, which was incident on the membrane, was 3.6×10^{-5} einsteins/s, measured using a radiometer (UDT, Model 380).

(*iii*) *Preparation of Colloidal Sols*

Sol–gel techniques were used to prepare four different precursor colloids. These sols were later used to prepare unsupported membranes or coated on glass supporting tubes, and then calcined to give ceramic membranes.

Colloid A (Nb-doped TiO_2 with a Ti/Nb mole ratio of 100 : 5). First, 5.73 g of $NbCl_5$ and 50 ml of absolute ethanol were mixed and stirred for 10 min. Then 125 ml of titanium tetraisopropoxide was added. This solution was stirred for an additional 10 min, then placed in an ice bath; 108 ml of a solution containing 7.6 ml of H_2O, 0.08 mol of HNO_3, and EtOH was added dropwise to the chilled solution. Subsequently, 750 ml of H_2O was added with vigorous stirring until a transparent solution formed. This solution

was then heated (while constantly being stirred) to 60°C and maintained at this temperature for 8 h, during which time a colloidal suspension formed. A rotary evaporator was used to remove enough solvent from the suspension to increase the solid's concentration to 4% by weight. The final pH of the suspension was 0.89 ± 0.05.

Colloid B (Nb-doped TiO_2 with a Ti/Nb mole ratio of 100:3). The preparation method was the same as that described for colloid A, except that the amounts of $NbCl_5$ and titanium tetraisopropoxide were adjusted to give the desired mole ratio. The resulting suspension contained 4% solids at pH 0.96 ± 0.05.

Colloid C (Pure TiO_2). This colloid was prepared by precipitation of TiO_2 produced by hydrolysis of titanium tetraisopropoxide. This step was followed by peptization with HNO_3 at 80°C (*24*). The resulting suspension contained 4% (w/w) titania at pH 1.32 ± 0.05.

Colloid D (Pure TiO_2). This colloid was prepared by hydrolysis of titanium tetraisopropoxide and peptization of the resulting precipitate with HNO_3 at room temperature. The nearly clear titania suspension at pH 1.35 ± 0.05 was then placed in a dialyzing membrane (Spectrum Medical Industries, Spectra/Por 3, MWCO:3 500) and immersed into 4 l of deionized water. Dialysis continued until the suspension pH reached 3.5 ± 0.1. Finally, the suspension was concentrated by removal of water to give a total solids concentration of 4% (w/w) and a pH of 3.35 ± 0.05.

(*iv*) *Preparation of Membranes*

Ceramic membranes were prepared in two forms: supported on glass (porous coatings) and unsupported.

Membranes supported on glass. The exterior surface of the inner glass (Pyrex) tube of the photochemical reactor was coated with TiO_2 using the following procedure. The tube, which had been sealed at one end, was immersed in the colloidal sol for 30 s, withdrawn at a controlled speed of 16.73 cm/min, and dried at room temperature for 1 h. This tube was then calcined in a furnace by heating from 100°C to the desired firing temperature (400, 500, or 600°C) at a rate of 3°C/min. It was then held at the firing temperature for 1 h. This protocol has the effect of depositing one layer of TiO_2 on the glass. To deposit additional layers, the entire process was repeated.

In order to measure several physical characteristics of supported membranes, glass plates (2.5 cm × 7.5 cm × 1.5 mm) were coated using the same protocol. In this case, TiO_2 membranes were deposited on both faces of the plates.

Unsupported membranes. Aliquots of the colloidal sols were placed in uncovered plastic containers and allowed to evaporate under controlled humidity conditions into air at room temperature. The resulting transparent xerogels were then fired following the same protocol used to prepare supported membranes. These unsupported ceramic membranes were crushed with an agate mortar and pestle to produce powders, which were characterized by different techniques.

(*v*) *Characterization of Membranes*

Surface areas, porosities, and pore size distributions of unsupported ceramic membranes were determined by physical adsorption of N_2. Specific surface area was calculated from the BET equation. Porosity was determined from the adsorption maxima. Pore size distributions based on the adsorption and the desorption branches of the isotherm were calculated using the Kelvin equation (*26*). The adsorption branch was used to obtain the modal size, given that it better represents the entire sample. The desorption branch overemphasizes the narrow sectors of the porous structure. Typical profiles of these pore size distributions have been presented elsewhere (*24, 25, 27*). It was verified that the modal pore size obtained by this procedure was in agreement with the corresponding value obtained by mercury porosimetry (*24*).

The average sizes of the primary particles in both supported and unsupported membranes were calculated from the peak widths at half-height obtained in X-ray diffraction (XRD) measurements at 25.4° or 27.5° in the case of anatase or rutile, respectively, using a Scintag, Inc., PAD V Diffraction System. These measurements also indicated that all of the supported membranes were composed of crystalline particles of anatase. For those unsupported TiO_2 membranes where both anatase and rutile phases were present, the average crystal size was calculated from peak area.

The thickness of the supported membranes was determined by profilometry (Tencor Instruments, alpha-step 200). Mobility measurements for the membrane precursor particles in the colloidal sols were performed on a PenKem System 3000 microelectrophoresis instrument in order to determine the isoelectric points of the different materials. Results are presented in Fig. 1, where mobility is represented vs pH. Isoelectric points are obtained from these curves for mobility equal to zero. These values are the following: colloid A, pH_{iep} = 5.4; colloid B, pH_{iep} = 5.7; and colloid C, pH_{iep} = 6.5.

The transmission of light through the membranes coated on glass plates was measured with a radiometer (UDT, Model 380). The light source used for this measurement was a 150-W Xe lamp enclosed in a metal chamber provided with an opening. Light from this source was passed through a monochromator and associated optics to give a beam with a cross-sectional area of 4 mm^2. The photodetector (1 cm^2 area) was placed just behind the coated glass plates. Since the incident light was normal to all interfaces (air–TiO_2–glass–TiO_2–air) the reflection coefficient was estimated for each change of medium according to

$$R = \frac{(n_1 - n_2)^2}{(n_1 + n_2)^2}, \qquad (1)$$

where R is the reflection coefficient and n_1 and n_2 are the refractive indices of the two media at each interface.

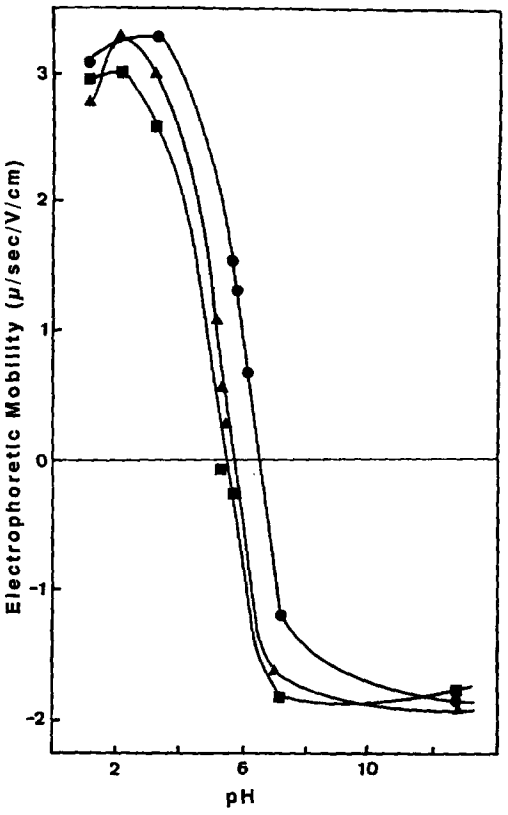

FIG. 1. Mobilities of precursor particles in the colloidal sol. Colloid: ■, A; ▲, B; ●, C.

The intensity of the light scattered by the membrane was calculated from measurements performed at 440 nm. At this wavelength light is not absorbed by TiO_2. For all the membranes used in these experiments this intensity was less than 4% of that of the incident light. The scattering measured at 440 nm is expected to be comparable to that for wavelengths between 300 and 400 nm. Measurements of light intensity always involved comparisons to blank experiments using uncoated glass plates. The absorption of light by the membranes was computed from the measured values of the reflected, transmitted, and scattered light intensities.

RESULTS AND DISCUSSION

(i) Physical–Chemical Characteristics

The physical–chemical characteristics of the membranes used to perform the photo-

TABLE 1

Characteristics of TiO_2 Ceramic Membranes

Membrane[a]	Firing temp. (°C)	Unsupported membranes				Supported membranes			
		Surface area (m^2/g)	Porosity (%)	Pore radius (Å)	Particle size (nm)	Particle size (nm)	Layers	Thickness (μm)	Absorbed/ Incident light[b]
A.1	400	125	28	17	6.0	8.6	6	1.1	0.52
A.2	500	88	25	19	13.0	11.4	6	1.0	0.56
A.3	600	33	19	13	20.0	13.0	6	1.0	0.56
B.1	400	130	29	17	6.5	8.3	6	1.1	0.45
B.2	500	50	20	20	14.7	—	6	1.1	0.48
B.3	600	8	11	—	33.3	—	6	1.2	0.47
C.1	400	140	31	17	6.8	8.1	6	1.1	0.32
C.2	500	2	3	—	30.0	14.6	6	1.0	0.36
C.3	600	≤0.1	≤0.1	—	46.9	26.6	6	1.1	0.38
D.1	400	168	45	25	7.2	4.6	9	0.9	0.35

[a] The letter in the label for each membrane indicates the precursor colloid from which it was prepared.
[b] For a wavelength of 365 nm.

degradation of 3-CSA are summarized in Table 1. For all the membranes fired at 400°C the values of the particle size, surface area, porosity and mean pore radius are quite similar, except for membrane D.1, which was prepared from the dialyzed colloid. This membrane has a significantly larger porosity and a larger mean pore radius, although its specific surface area is comparable to those of the other membranes. These physical differences are believed to result from the dialysis process. Continuous withdrawal of protons, the potential-determining ions for the particles, from the suspension causes the formation of aggregates with loose structures. These aggregates, which have relatively large pores and pore volumes, tend to retain their porous structure during gelation. Additional details concerning these membranes have been presented elsewhere (*28*).

As the firing temperature is increased, sintering of the membrane occurs. In the early stages of sintering, grain growth and a small amount of linear shrinkage take place. These phenomena are reflected by the increase in the primary particle size and the decrease in specific surface area (and porosity), respectively. This is depicted in Fig. 2A, where specific surface area (S_g) has been plotted vs particle size for unsupported membranes. The specific surface area decreases exponentially as particle size increases, accordingly with the following equation,

$$S_g = a\, e^{-bD_p}, \qquad (2)$$

where

$$a = 258 \pm 0.2\ m^2/g$$
$$b = -0.103 \pm 0.019\ nm^{-1}$$

for membranes A (5% Nb) and B (3% Nb), and

$$a = 471 \pm 0.2\ m^2/g$$
$$b = -0.18 \pm 0.02\ nm^{-1}$$

for membrane C (pure TiO_2) Figure 2B is a representation of the linearized form of Eq. (2). The solid line in Fig. 2A represents an equivalent specific surface area (S_e); that is, the specific surface area of equivalent spherical particles if they were separated from one another. This equivalent specific surface area is determined by the well known equation

$$S_e = \frac{6}{\rho D_p}, \qquad (3$$

where $\rho = 3.9\ g/cm^3$ is the density of TiO

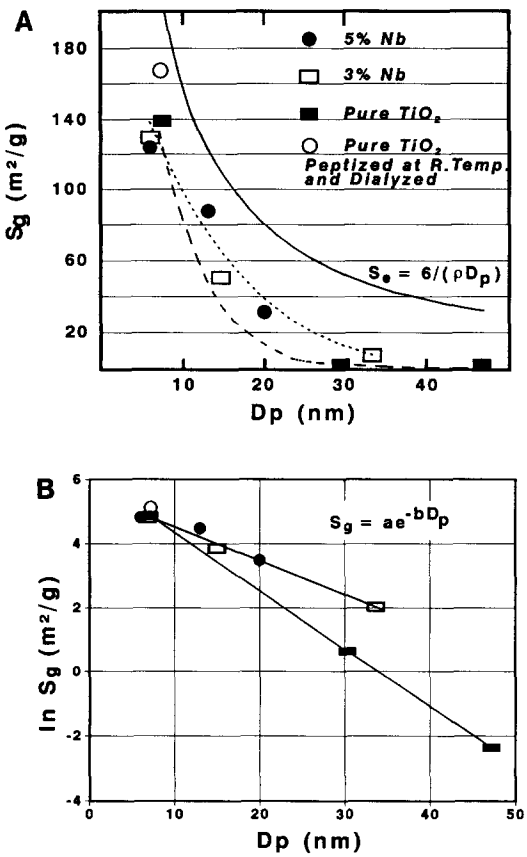

FIG. 2. Evolution of specific surface area (S_g) vs particle diameter (D_p) as membrane firing temperature increases from 400 to 600°C (from left to right; see Table 1). Unsupported membranes: ●, A(5% Nb); □, B(3% Nb); ■, C(pure TiO_2), ○, D(pure TiO_2). (A) The dotted lines are curves fitted to the equation $S_g = ae^{-bD_p}$; the solid line is the equivalent specific surface area (S_e). (B) Plot of the linearized equation.

As expected, the evolution of S_g as membranes are fired falls below S_e. The difference $S_e - S_g$ corresponds to grain boundaries and closed pores in the membranes.

The increase in mean pore radius with an increase in firing temperature from 400 to 500°C has consistently been observed in our studies of ceramic membranes (*24, 25*). Our interpretation of this observation is that as hydroxyl groups desorb from the pore walls when the firing temperature is increased, the large pores increase in size while the small pores collapse. The thermal removal of water and hydroxyl groups and its significance for photo-induced processes at TiO_2 surfaces have been pointed out by several authors in detailed studies (*29, 30*). In the particular case of TiO_2 membranes, adsorption studies carried out in our laboratory with salicylate anions (*31*) revealed a decrease in adsorption (mol/g) with increasing firing temperature. However, when the adsorption isotherms were normalized with respect to the surface area (mol/m^2), data for all these membranes fit on the same isotherm. Therefore, the decrease in adsorption with increasing firing temperature seems to be related directly to a decrease in the numbers of titanium cations and hydroxyl groups present per unit area available for bonding.

At higher sintering temperatures, shrinkage is greatly accelerated, since the sintering process is then dominated by viscous flow effects arising from the thermodynamic forces striving to minimize the surface energy of the system. Surface area and porosity drop rapidly to zero, all the pores close, and a densified material is produced. In the case of the membrane prepared from colloid A, the data in Table 1 indicate that the pores start to close at 600°C. Unfortunately, pore radii could not be determined for other membranes fired at 600°C, as their specific surface areas were less than 20 m^2/g.

Note that both doping of membranes with Nb and placing membranes on supports act to limit the physical changes that occur in the membranes as they are heated. If membranes fired at different temperatures are compared, changes in surface area, porosity and pore size are more drastic for pure TiO_2 membranes (C) than they are for Nb-doped TiO_2 membranes (A and B). When pure TiO_2 membranes are fired at 600°C, less than 0.1% of the original surface area remains, and the porosity decreases dramatically. At the same time the mean particle size increases greatly.

If the mean particle sizes for the supported and unsupported membranes are

compared as the firing temperature for the membranes is increased, the particles constituting the unsupported membranes grow much faster than do those of the supported membrane. Evidence obtained in our laboratory indicates that unsupported TiO_2 membranes fired at 500°C are partially converted to the rutile crystalline form, while unsupported membranes fired at 600°C are converted completely to rutile (*31, 32*). The transition temperature appeared to be in the range 475–500°C (*31*). However, supported membranes fired at these temperatures remain in the anatase form (*32*). These observations suggest that it is more difficult for particles attached to a support to sinter or convert to other crystalline forms than it is for particles in unsupported membranes to undergo these processes. Thus, for supported membranes, changes in surface area, porosity, and pore radius should not be as drastic as those for unsupported membranes (see Table 1). However, measurements performed on unsupported membranes can at least provide a relative indication as to how the sintering protocol used to prepare supported membranes affects the physical–chemical properties of those membranes.

(*ii*) *Photoefficiency*

The complete dechlorination of 3-CSA was demonstrated in a previous work (*21*). An ion selective electrode was employed to determine the chloride ion concentration. In experiments where the reaction proceeded to near completion, the amounts of HCl produced were always >98% of the 3-CSA which disappeared. Production of CO_2 was demonstrated by observing the precipitation of $BaCO_3$ in the $Ba(OH)_2$ solution used to scrub the effluent gas stream. More recently (*33*), in experiments where 3-CSA was analyzed by HPLC, the ratio (3-CSA consumed)/(HCl produced) was constant, ca. 1, as the reaction proceeded. Furthermore, total organic carbon measurements indicated that 3-CSA had completely been mineralized.

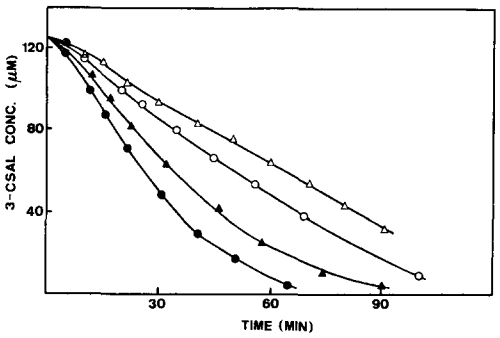

FIG. 3. Degradation of 3-chlorosalicylic acid with membranes fired at 400°C, pH 6. Membrane: ○, A.1; △, B.1; ▲, C.1; ●, D.1.

Initial experiments were performed to determine the effect of TiO_2 coating layers on the degradation rate. For all membranes fired at 400°C, the photoactivity initially increased as the number of layers increased. However, plateaus were reached after six layers for membranes A.1, B.1, and C.1, and after nine layers for membrane D.1. Supports coated with enough layers to reach these plateau values were used in subsequent studies.

For the membranes fired at 400°C, Fig. 3 depicts the decrease in the concentration of 3-CSA concentration as illumination time increases. Pseudo-first-order kinetic constants and quantum yields are summarized in Table 2. Membrane D.1 produced the fastest degradation. Nb-doped membranes (A.1 and B.1) were less active than the pure TiO_2 membranes (C.1 and D.1). To analyze the effect of Nb-doping, one should compare membranes prepared by the same sol–gel technique, i.e., A.1, B.1., and C.1.

Doping reduces the effective bandgap. The dopant energy level makes it appear that the effective bandgap is less than the actual bandgap of TiO_2. When the dopant is from a neighboring group of the Periodic Table, it increases the electrical conductivity. The dark conductivity of unsupported pure and Nb-doped membranes was measured using a standard four-probe dc technique (*34*). Results and discussion have

TABLE 2
Pseudo-first-order Kinetic Constant (k) and Quantum Yield for the Degradation of 3-CSA Using Different TiO_2 Ceramic Membranes

Membrane	pH	k^a ($\times 10^4$ s^{-1})	Q.Y.^{b} (%)
A.1	4.3	2.89	0.15
A.1	6	2.42	0.13
A.2	6	2.31	0.11
A.3	6	1.35	0.07
B.1	6	2.08	0.13
B.2	6	1.96	0.11
B.3	6	1.26	0.07
C.1	4.3	4.28	0.37
C.1	6	3.76	0.33
C.2	6	3.68	0.28
C.3	6	2.89	0.21
D.1	6	4.65	0.37

[a] Values calculated at 3-CSA concentration 100 μM.
[b] Quantum Yield: (Reaction rate, mol/s)/(Absorbed light, einstein/s).

been presented elsewhere (*32*). Conductivity increased drastically with Nb doping and reached a plateau about 5 mole %. This increase is considered to be due to Nb^{4+}, which behaves as an electron donor (*35*).

Semiconductors with smaller bandgap energies utilize a wider range of the light spectrum and have greater optical absorption at each wavelength. Thus, for the same membrane thickness and porosity, Nb-doped TiO_2 membranes absorb more light than pure TiO_2 membranes (see Table 1). The higher electric conductivity observed for Nb-doped membranes indicates that, in doped membranes, less time is necessary for electrons and holes to reach the catalyst surface where they can induce photodecomposition reactions. Both these effects should improve the photocatalytic properties of Nb-doped TiO_2 membranes relative to pure TiO_2 membranes. However, Nb-doping will also affect the rate at which electron–hole recombination processes occur in the catalyst. If the radiationless recombination rate increased on doping, then the reaction efficiency would decrease. The data in Fig. 3 seem to indicate that this is the case.

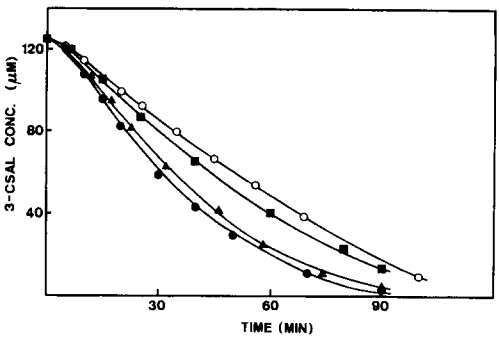

FIG. 4. Effect of pH on the rate of degradation of 3-chlorosalicylic acid over membranes fired at 400°C. Membrane: ■, A.1 (pH 4.3); ○, A.1 (pH 6); ●, C.1 (pH 4.3); ▲, C.1 (pH 6).

Another factor that can influence the rate of the degradation reaction is the surface charge on the membrane. This parameter is important in determining the propensity for 3-CSA to adsorb on the membrane. Since 3-CSA exists completely in the anionic form at pH 6, adsorption will be favored on surfaces bearing a positive charge.

The mobilities of the particles in the precursor colloidal sols are shown as functions of pH in Fig. 1. Note that at pH 6, the pure TiO_2 surface bears a positive charge while the Nb-doped TiO_2 bears a negative charge. Because 3-chlorosalicylate ions would more readily adsorb on pure TiO_2 surfaces than on Nb-doped surfaces, photodegradation on pure TiO_2 should be faster. To test this hypothesis, kinetic studies were performed at pH 4.3, where the membrane surfaces are all positive. The results depicted in Fig. 4 indicate that the degradation occurs more rapidly at pH 4.3 than at pH 6. It should be noted that, at pH 4.3, the protonated form of 3-CSA is not negligible, but the predominant species is still the anionic form.

This is in agreement with the results of a previous work devoted specifically to a study of the relation between adsorption and the photodecomposition rate (*31*) where unsupported pure TiO_2 ceramic membranes were used. It was found that the adsorption densities of 3-CSA decreased with both in-

creasing solution pH and membrane firing temperature. Likewise, the photodegradation rate of 3-CSA also diminished with increasing pH.

For all the membranes studied, photodegradation at pH 4.3 was slightly faster than at pH 6. Nonetheless, the pure TiO_2 membrane was still more efficient than either Nb-doped membrane. This observation suggests that the different surface charges on pure TiO_2 and Nb-doped TiO_2 at pH 6 are not primarily responsible for the higher activity of pure TiO_2. Therefore, a larger rate for e^-/h^+ recombination processes seems to be the most logical explanation for the lower degradation efficiency observed with Nb-doped TiO_2 membranes relative to pure TiO_2 membranes.

In an earlier work, where the photoelectrochemical properties of Nb-doped TiO_2 ceramic membranes were studied (*32*), it was observed by using a hole scavenger (EtOH) that the larger increases of photocurrent corresponded to those membranes with the most grain boundaries. These increases were also higher for doped membranes, when compared with undoped membranes fired at same temperature. Both facts seem to support the idea of an enhancement of e^-/h^+ recombination at dopant centers and at grain boundaries, where the mismatch of crystal domains can be regarded as crystal defects. Bulk recombination at point defects and dislocations has been analyzed and is well documented ((*36*) and citations therein).

The effect of firing temperature on the photocatalytic activity of the membrane is indicated in Fig. 5 and Table 2. Results obtained with membranes fired at 400°C were not included in Fig. 5. The specific surface area seems to play a key role in determining the efficiency of the degradation process. In a previous kinetic study (*21*), it was found that a rate law of the general Langmuir–Hinshelwood–Hougen–Watson form was consistent with kinetic data. The rate equation was developed from a reaction mechanism that involves the adsorption of 3-CSA and

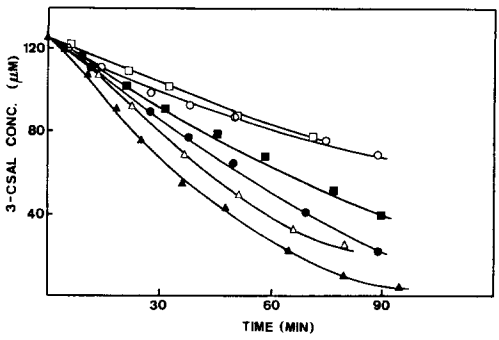

FIG. 5. Effect of firing temperature on the degradation of 3-chlorosalicylic acid, pH 6. Membrane: ●, A.2; ■, B.2; ▲, C.2; ○, A.3, □, B.3; △, C.3.

oxygen on the surface. Therefore, the availability of surface sites is crucial for the process. Unfortunately, the specific surface areas of the supported membranes are not known. However, a rough estimate can be inferred based on the particle size values measured for the supported membranes and the use of the appropriate form of Eq. (2) for doped and undoped membranes, respectively. These equations have been derived for unsupported membranes. However, the structural changes in the corresponding supported membranes when fired could evolve following paths close to those represented in Fig. 2, though retarded by the support.

Figure 6A is a plot of the natural logarithm of quantum yield (Q.Y.) divided by specific surface area (S_g) vs particle size (D_p). As shown, the undoped membrane C when fired (increasing D_p) follows a linear path with positive slope. This is in agreement with the hypothesis of the e^-/h^+ recombination at grain boundaries, for the area of the grain boundaries decreases and membrane crystallinity increases as particles grow with firing temperature. Nb-doped membranes behave in a different manner, the ratio QY/S_g being independent of D_p. This would be expected if recombination at point defects created by doping was comparatively much greater than that at grain boundaries.

Figure 6B an illustration of the evolution of quantum yield with the ratio specific sur-

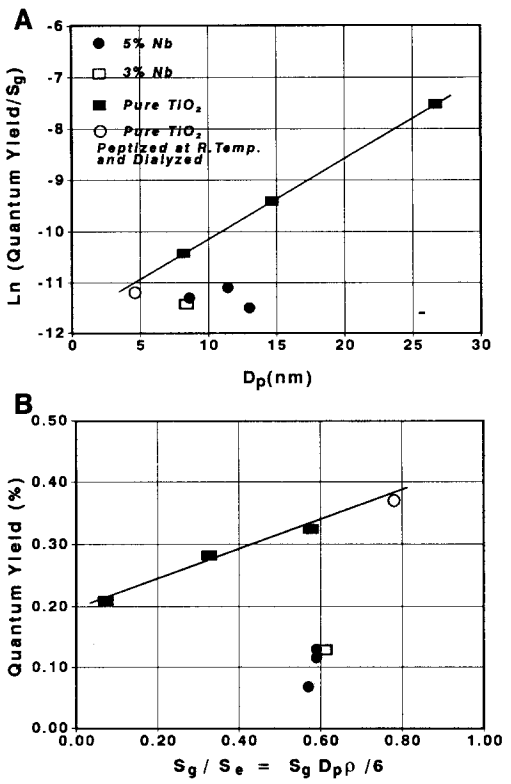

FIG. 6. Correlations of quantum yield (Q.Y.) vs specific surface area (S_g) and particle size (D_p). Membranes: ●, A(5% Nb); □, B(3% Nb); ■, C(pure TiO_2); ○, D(pure TiO_2). (A) Effect of raising firing temperature (increasing D_p) on the ratio Q.Y./S_g. (B) Quantum yield vs the ratio (S_g/S_e). $S_e = 6/\rho D_p$ is the equivalent specific surface area. (Firing temperature increases from the right to the left).

face area/equivalent specific surface area (S_g/S_e). If Eq. (2) and (3) are taken into account,

$$\frac{S_g}{S_e} = \frac{\rho D_p S_g}{6} = \frac{a\rho D_p e^{-bD_p}}{6}. \qquad (4)$$

Therefore, Figure 6B is another way of correlating the same variables, Q.Y. and D_p. As D_p increases with firing temperature, the ratio S_g/S_e decreases and so does the quantum yield. It illustrates once again the relevance of S_g for the efficiency of this process and, in addition, the importance of having a ratio S_g/S_e close to unity. As this ratio approaches unity, the proportion between specific surface area and grain boundaries and closed pores increases dramatically. The increase of S_g enhances the amount of charge scavengers in the membrane that can restrain e^-/h^+ recombination. This seems particularly crucial in Nb-doped membranes, where the density of bulk defects is much higher. Membrane D, undoped, with the highest S_g and S_g/S_e values, gives the best efficiency.

CONCLUSIONS

—TiO_2 ceramic membranes supported on glass are able to bring about the complete mineralization of 3-CSA, a halogenated aromatic compound.

—Both doping the TiO_2 membranes and coating the membranes on a support limit changes in the physical–chemical characteristics of these ceramic membranes when they are fired at high temperatures.

—Doping with niobium improves the light absorbance of membranes. However, the rate of the degradation of 3-CSA is not improved.

—The growth of membrane particles as firing temperature is increased produces an exponential reduction in specific surface area. As a result, the efficiency of the membrane decreases substantially. The efficiency decline is more marked in the Nb-doped membranes.

—An explanation based on the hypothesis of e^-/h^+ recombination at flaws and point defects of the membranes seems to account for these facts.

ACKNOWLEDGMENTS

This work has been supported in part by grants from the USDOE (Contract DE-AS07-86ID12626), USDOE Savannah River Facility (Contract AX0798826-1), USEPA (Contract R813457-01-0), and Babcock–Hitachi K.K.; and by grants from CIRIT (Generalitat de Catalunya, Spain) and DGICYT (Ministerio de Educación y Ciencia, Spain).

REFERENCES

1. Graetzel, M. (Ed.), "Energy Resources through Photochemistry and Catalysis." Academic Press, New York, 1983.
2. Schiavello, M. (Ed.), "Photoelectrochemistry,

Photocatalysis and Photoreactors." Reidel, Dordrecht, 1985.
3. Gruzdkov, Yu. A., Savinov, E. N., and Parmon, V. N., *Int. J. Hydrogen Energy* **12,** 393 (1987).
4. Escudero, J. C., Gimenez, J., Simarro, R., and Cervera-March, S., *Sol. Energy Mater.* **17,** 151 (1988).
5. Gimenez, J., Escudero, J. C., Sabate, J., Simarro, R., and Cervera-March, S., *Hydrogen Energy Prog.* **7,** 299 (1988).
6. Sabate, J., Cervera-March, S., Simarro, R., and Gimenez, J., *Int. J. Hydrogen Energy* **15,** 115 (1990).
7. Frank, S. N., and Bard, A. J., *J. Am. Chem. Soc.* **99,** 303 (1977).
8. Nguyen, T., and Ollis, D. F., *J. Phys. Chem.* **88,** 3386 (1984).
9. Ollis, D. F., Hsiao, C. Y., Budiman, L., and Lee, C. L., *J. Catal.* **88,** 89 (1984).
10. Tunesi, S., and Anderson, M. A., *Chemosphere* **16,** 1447 (1987).
11. Barbeni, M., Pramauro, E., Pelizzetti, E., Borgarello, E., and Serpone N., *Chemosphere* **14,** 195 (1985).
12. Buhler, N., Meier, K., and Reber, J., *J. Phys. Chem.* **88,** 3261 (1984).
13. Reber, J. F., and Meier, K., *J. Phys. Chem.* **88,** 5903 (1984).
14. Reber, J. F., and Rusek, M., *J. Phys. Chem.* **90,** 824 (1986).
15. Serpone, N., Borgarello, E., Barbeni, M., and Pelizzetti, E., *Inorg. Chim. Acta* **90,** 191 (1984).
16. Serpone, N., Borgarello, E., Pelizzetti, E., and Barbeni, M., *Chim. Ind. (Milan)* **67,** 318 (1985).
17. Esplugas, S., Cervera-March, S., and Simarro, R., *Chem. Eng. Commun.* **51,** 221 (1987).
18. Serpone, N., Borgarello, E., Harris, R., Cahill, P., and Pelizzetti, E., *Sol. Energy. Mater.* **14,** 121 (1986).
19. Matthews, R. W., *J. Phys. Chem.* **91,** 3328 (1987).
20. Matthews, R. W., *J. Catal.* **111,** 264 (1988).
21. Sabaté, J., Anderson, M. A., Kikkawa, H., Edwards, M., and Hill, C. G., Jr., *J. Catal.* **127,** 167 (1991).
22. Sakka, S., and Kamiya, K., *J. Non-Cryst. Solids* **48,** 31 (1982).
23. Sakka, S., *Am. Ceram. Soc. Bull.* **64,** 1463 (1985).
24. Anderson, M. A., Gieselmann, M. J., and Xu, Qunyin, *J. Membr. Sci.* **39,** 243 (1988).
25. Gieselmann, M. J., Anderson, M. A., Moosemiller, M. D., and Hill, C. G. Jr., *Sep. Sci. Technol.* **23,** 1715 (1988).
26. Hiemenz, P. C., "Principles of Colloid and Surface Chemistry." Dekker, New York, 1977.
27. Xu, Q., and Anderson, M. A., *Mater. Res. Soc. Symp. Proc.* **132,** 41 (1989).
28. Xu, Q., and Anderson, M. A., *J. Mater. Res.* **6,** 1073 (1991).
29. Munuera, G., Rives-Arnau, V., and Saucedo, A., *J. Chem. Soc., Faraday Trans. 1* **75,** 736 (1979).
30. Bickley, R. I., Jayanty, R. K. M., Vishwanathan, V., and Navio, J. A., *in* "Homogeneous and Heterogeneous Photocatalysis" (E. Pelizzetti and N. Serpone, Eds.), Reidel, Dordrecht, 1986.
31. Tunesi, S., and Anderson, M. A., *J. Phys. Chem.* **95,** 3399 (1991).
32. Kikkawa, H., O'Regan, B., and Anderson, M., submitted for publication.
33. Kottelat, J. P., and Anderson, M. A., in preparation.
34. Van Pauw, L. J., *Philips Res. Rep.* **13,** 1 (1958).
35. Salvador, P., *Sol. Energy Mater.* **2,** 413 (1980).
36. Morrison, S. R., "Electrochemistry at Semiconductor and Oxidized Metal Electrodes." Plenum Press, New York, 1984.